JGR Oceans

RESEARCH ARTICLE
10.1029/2018JC014928

Impact of Near-Inertial Waves on Vertical Mixing and Air-Sea CO_2 Fluxes in the Southern Ocean

Hajoon Song[1], John Marshall[2], Jean-Michel Campin[2], and Dennis J.McGillicuddy Jr.[3]

[1]Department of Atmospheric Sciences, Yonsei University, Seoul, South Korea, [2]Department of Earth, Atmospheric and Planetary Sciences, Massachusetts Institute of Technology, Cambridge, MA, USA, [3]Department of Applied Ocean Physics and Engineering, Woods Hole Oceanographic Institution, Woods Hole, MA, USA

Abstract We report the significant impact of near-inertial waves (NIWs) on vertical mixing and air-sea carbon dioxide (CO_2) fluxes in the Southern Ocean using a biogeochemical model coupled to an eddy-rich ocean circulation model. The effects of high-frequency processes are quantified by comparing the fully coupled solution (ONLINE) to two offline simulations based on 5-day-averaged output of the ONLINE simulation: one that uses vertical mixing archived from the ONLINE model (CTRL) and another in which vertical mixing is recomputed from the 5-day average hydrodynamic fields (5dAVG). In this latter simulation, processes with temporal variabilities of a few days including NIWs are excluded in the biogeochemical simulation. Suppression of these processes reduces vertical shear and vertical mixing in the upper ocean, leading to decreased supply of carbon-rich water from below, less CO_2 outgassing in austral winter, and more uptake in summer. The net change amounts up to one third of the seasonal variability in Southern Ocean CO_2 flux. Our results clearly demonstrate the importance of resolving high-frequency processes such as NIWs to better estimate the carbon cycle in numerical model simulations.

Key Points:
- Filtering out near-inertial waves diminishes vertical shear and hence mixing, shallowing the mixed layer depth in a model simulation
- The shallowed mixed layer reduces the supply of dissolved inorganic carbon to the surface
- Near-inertial-waves-induced mixing can change the air-sea CO_2 flux by one-third amplitude of the seasonal cycle

Supporting Information:
- Supporting Information S1
- Text S1
- Figure S1
- Figure S2
- Figure S3

Correspondence to:
H. Song,
hajsong@yonsei.ac.kr

Citation:
Song, H., Marshall, J., Campin, J.-M., & McGillicuddy, D. J. (2019). Impact of near-inertial waves on vertical mixing and air-sea CO_2 fluxes in the Southern Ocean. *Journal of Geophysical Research: Oceans*, *124*, 4605–4617. https://doi.org/10.1029/2018JC014928

Received 3 JAN 2019
Accepted 10 JUN 2019
Accepted article online 17 JUN 2019
Published online 8 JUL 2019

1. Introduction

Intensive vertical mixing is one of the important aspects that characterize the Southern Ocean (SO; de Boyer Montégut et al., 2004; Holte et al., 2017). To the north of the Antarctic Circumpolar Current (ACC), thick mixed layers in austral winter reach a few hundred meters deep and contribute to the exchanges of momentum, heat, and freshwater, and formation of Antarctic Intermediate Water and Subantarctic Mode Water (Dong et al., 2008). Deep vertical mixing is also important in biogeochemical processes. It brings surface water, rich in oxygen, to the interior ocean during the process of intermediate and mode water formations and forms the oxygen maximum layer (Talley et al., 2011). The uptake of anthropogenic tracers (e.g., chlorofluorocarbons) can be expedited through deep convection (Shao et al., 2013; Song et al., 2015). Intensive vertical mixing is also efficient in drawing the subsurface water mass rich in nutrients and carbon close to the surface. For example, iron, critical for the primary production in the SO, is supplied from the interior of the ocean by vertical mixing in winter (Tagliabue et al., 2014). Vertical mixing may also be responsible for the nitrate transport from the deep Eastern South Pacific to the Patagonian shelf region that is one of the most productive areas in the world (Song, Marshall, Follows, Dutkiewicz & Forget, 2016).

Near-inertial waves (NIWs) can significantly impact surface vertical mixing. They have a frequency close to an inertial frequency with a length scale of 10 to 100 km and are mainly excited by wind forcing (Alford et al., 2016). In particular, midlatitude storms can drive the ocean with their inertially rotating components (D'Asaro, 1985) and excite high and low mode waves. High modes create counterclockwise rotation in the SO, producing high vertical shear of currents and enhanced vertical mixing along with downward propagation of energy (Alford & Gregg, 2001; Alford et al., 2016). In numerical experiments, NIWs deepen mixed layer depths (MLDs) by up to 30% on the annual average between 40°S and 60°S (Jochum et al., 2013). This deepening of MLDs in the SO is associated with the midlatitude storm tracks (Simmons & Alford, 2012), which is consistent with the view that a high level of wind work can generate NIWs.

The modulation of vertical mixing by NIWs is expected to influence air-sea CO_2 exchange in the SO. The SO CO_2 flux is controlled by two key processes: biological drawdown and intensive vertical mixing (Takahashi et al., 2009; Wetzel et al., 2005). In austral summer, the SO takes up CO_2 from the atmosphere with biological

processes leading to drawdown, but it emits CO_2 into the atmosphere in austral winter due to the entrainment of carbon-rich interior water up to the surface. It is thus anticipated that enhanced vertical mixing by NIWs promotes more entrainment in austral winter, resulting in more CO_2 outgassing. However, it is not well investigated how much these processes influence air-sea CO_2 exchange. In addition, their role in austral summer is uncertain as biological drawdown is itself impacted by the MLD. Deepening of the MLD in austral summer may enrich the surface ocean with carbon while bringing more nutrients to the surface that potentially promote higher biological drawdown. Although cooling of the surface water due to enhanced mixing increases the solubility and lowers the partial pressure of CO_2 (pCO), which leads to higher CO_2 uptake, it is difficult to anticipate the net effect of high-frequency processes on the CO_2 flux.

Here we attempt to quantify the integral effect of NIWs on CO_2 flux near Drake Passage in the SO. Our approach is to compare CO_2 fluxes with and without high temporal variabilities including NIWs by making use of both online and offline biogeochemical models. The online biogeochemical simulation is forced by 6-hourly winds to capture the input of energy with near-inertial frequency. The offline biogeochemical simulation is forced by the same wind forcing, but the ocean states driving biogeochemical variables are the 5-day-averaged fields from the online simulation, as described in section 2. The results in section 3 suggest that high-frequency effects are capable of altering the air-sea CO_2 flux significantly through changes in the vertical flux of carbon. A discussion on air-sea CO_2 simulation follows in section 4.

2. Simulations of Air-Sea CO_2 Flux

2.1. Eddy-Resolving Model

A simple biogeochemical model (Dutkiewicz et al., 2005; Parekh et al., 2006; Verdy et al., 2007) is coupled to a 1/20° version of the MIT Ocean General Circulation Model (MITgcm; Adcroft, Hill, Campin et al., 2004; Adcroft, Hill & Marshall 1997; Marshall, Adcroft, et al., 1997; Marshall, Hill, et al., 1997; Marshall et al., 1998). The model domain covers the area from −75°S to −35°S with a 140° longitudinal swath of a section of the ACC stretching from the Southeast Pacific through Drake Passage to the Southwest Atlantic (Figure 1a) and deploys 50 vertical levels with higher resolution near the surface (10 m). The model configuration is as described in Tulloch et al. (2014) and the same as that used in Song, Marshall, Munro, Dutkiewicz, Sweeney, et al. (2016). In particular, the ocean model was integrated with 6-hourly wind and buoyancy fluxes from the reanalysis data set by European Centre for Medium-Range Weather Forecasts (Simmons et al., 2007). Vertical mixing is parameterized by the nonlocal K-profile parameterization (KPP) scheme of Large et al. (1994) in which the depth of the boundary layer is first estimated based on the bulk Richardson number determined by the surface forcing, buoyancy, and vertical velocity shear. The vertical diffusivity is calculated within the boundary layer scaled with its depth. In our experiment, the mixing depth is from the surface to the level where the Richardson number is less than 0.3583. We treat the mixing depth as MLD in our analysis. The biogeochemical boundary conditions are provided from the monthly mean states from a global model (Song, Marshall, Munro, Dutkiewicz, Sweeney, et al., 2016). The integration of this configuration (referred to as ONLINE hereinafter) for 4 years with a time step of 2 min results in ocean states that have close similarities to the observed SO states including a high level of mesoscale eddy activities whose spatial scale is O(100 km).

The existence of the NIWs is verified using rotary spectra. The rotary spectra reveal the frequency and power of the rotational motion. When the horizontal current is written in complex form, we can compute the fast Fourier transformation to find out the power at both positive and negative frequencies. The positive frequencies show the clockwise rotational motion, while the negative frequencies are for the counterclockwise rotational motion. In the rotary spectra of velocity shear at 100 m, there are two distinct lines with elevated power at each latitude: one for the frequency band near zero and the other close to the inertial frequency (Figure 2a). While the former is associated with geostrophic flow, the latter reveals NIWs. Velocity shear rotates counterclockwise with positive frequencies near-inertial frequency, f. The rotary spectra of velocity also show enhanced variance near f as well as at low frequency (Figure S1 in the supporting information), consistent with that obtained from drifter velocity observations (Elipot & Lumpkin, 2008; Elipot et al., 2016). The wavenumber spectrum using the surface current has a slope close to k^{-3}, with k being the wavenumber (Figure 2c). This suggests that mesoscale eddies derive their energy source from baroclinic instability (Sasaki et al., 2014).

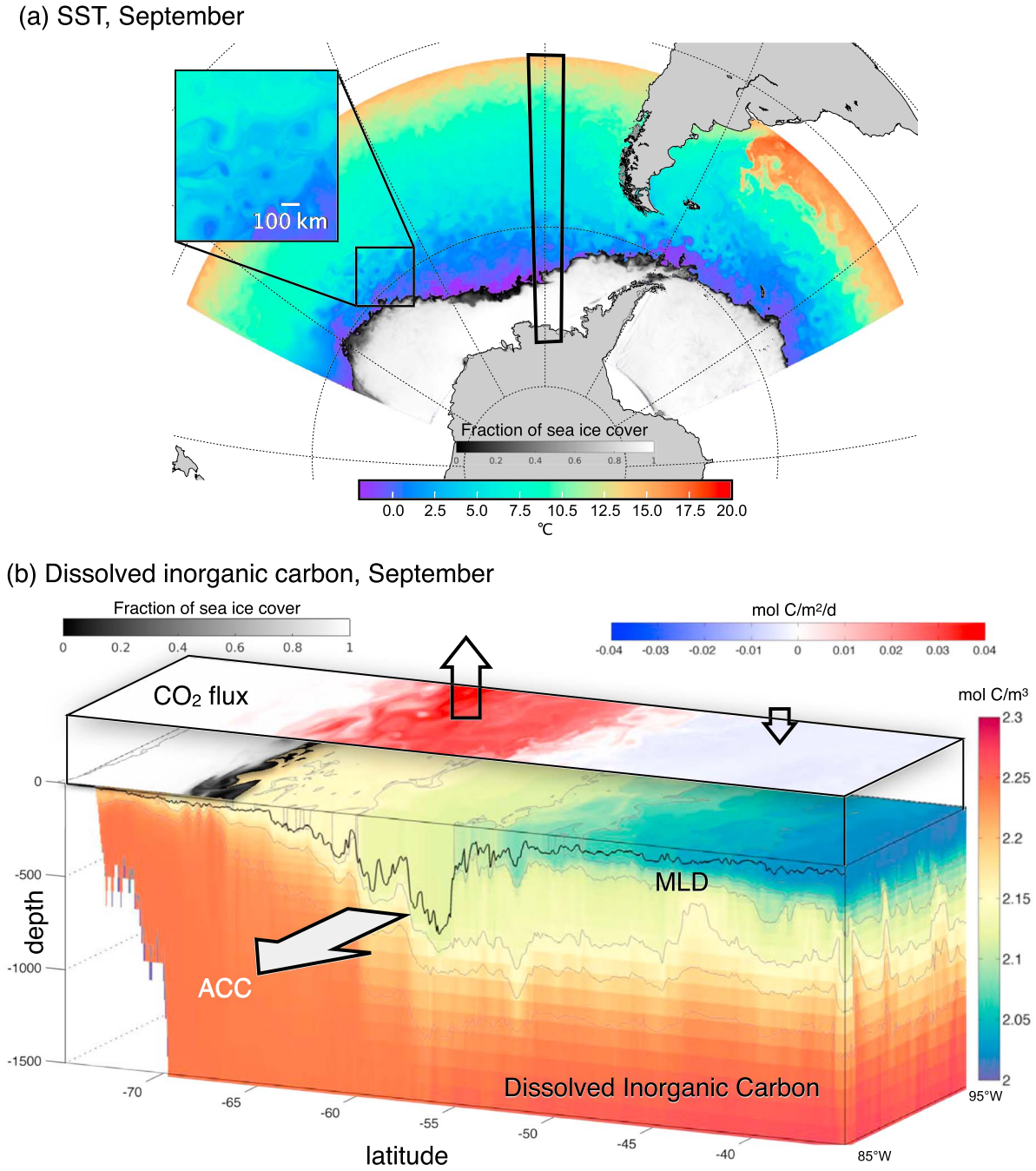

Figure 1. (a) A snapshot of sea surface temperature (SST) from the online simulation (ONLINE) in September. The mask in the gray color scale around Antarctica represents the sea ice concentration. The rectangular box at the center indicates the region of the vertical section of dissolved inorganic carbon from the surface to 1,500 m in (b). Dissolved inorganic carbon and air-sea CO_2 flux. The thin black line in (b) marks the mixed layer depth (MLD) defined as the level whose density is 0.03 kg/m^3 greater than the surface value. The air-sea CO_2 flux is represented at the surface by colors and the vertical arrows. The mask in the gray color scale at the surface is the sea ice concentration. The direction of the Antarctic Circumpolar Current (ACC) is shown as a gray arrow in (b).

2.2. Simulation of Air-Sea CO_2 Flux

The air-sea CO_2 flux (F_{CO_2}) is estimated using a gas exchange parameterization:

$$F_{CO_2} = K_w \left(1 - A_{SI}\right) \left(pCO_2 - pCO_2^{atm}\right), \quad (1)$$

where K_w is the gas transfer velocity (m/s) determined by wind speed squared and sea surface temperature (Wanninkhof, 1992), A_{SI} is the fraction of the sea ice coverage within a model grid cell varying from 0 when

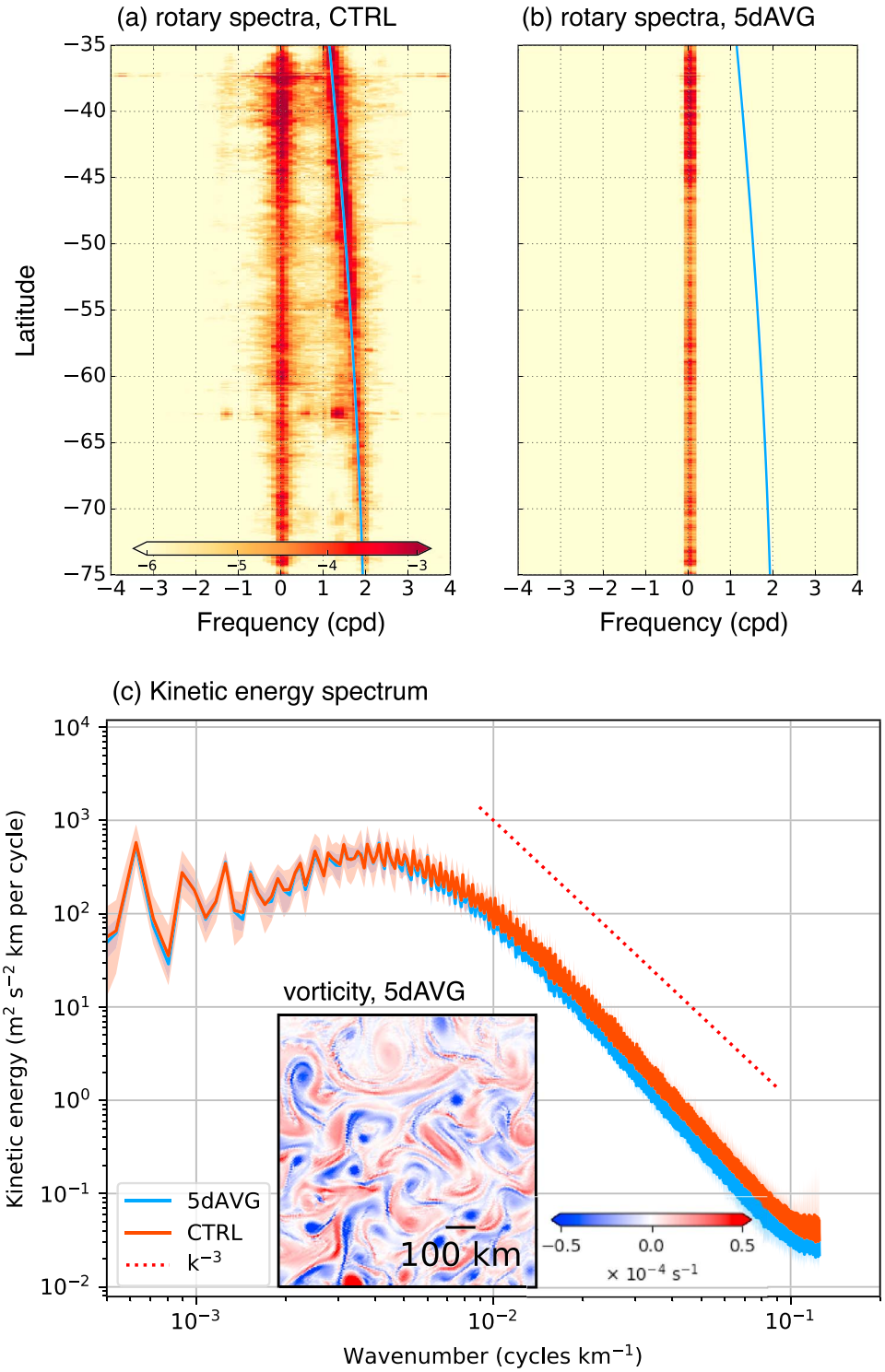

Figure 2. The rotary spectra of vertical shear (s^{-2}·cpd^{-1}) using a $\log_{10}$ scale at 100 m in the (a) 1/20° eddy-resolving model and (b) 5-day-averaged velocity. Blue lines in (a, b) represent the inertial frequency, $-f/(2\pi)$, where f is the Coriolis frequency. The kinetic energy spectra of the surface current in ONLINE (red) and 5dAVG (blue) are plotted in (c). Shading indicates the maximum/minimum energy levels during the last 3-year simulation. The inset in (c) is the surface vorticity from 5dAVG.

Table 1
Comparison of Biogeochemical Simulations

Name	ONLINE	CTRL	5dAVG
Biogeochemical coupling method to circulation/physics	online	offline	offline
Physical fields	T, S, u, and v	$\langle T\rangle$, $\langle S\rangle$, $\langle u\rangle$, and $\langle v\rangle$	$\langle T\rangle$, $\langle S\rangle$, $\langle u\rangle$, and $\langle v\rangle$
Eddy diffusivity (κ) in the KPP scheme	computed using T, S, u, and v	$\langle\kappa\rangle$ from ONLINE is loaded.	computed using $\langle T\rangle$, $\langle S\rangle$, $\langle u\rangle$, and $\langle v\rangle$

Note. In the table, T, S, u, and v represent a snapshot of temperature, salinity, zonal velocity, and meridional velocity, respectively, with a frequency of 120 s. The 5-day average of those variables are written using angled bracket, $\langle\rangle$.

there is no sea ice to 1 when the grid cell is fully covered by sea ice, and pCO_2 and pCO_2^{atm} are the oceanic and atmospheric partial pressures of CO_2, respectively. We fix pCO_2^{atm} at the preindustrial level (278 ppm), and oceanic surface pCO_2 is estimated using dissolved inorganic carbon (DIC), alkalinity, and temperature and salinity, following Follows et al. (2006).

The distribution of DIC in austral winter reveals the upwelling that increases the surface DIC on the poleward side of the ACC (Figure 1b). Near Antarctica where the surface DIC is the greatest, the CO_2 outgassing is inhibited by the presence of sea ice. Instead, the strongest CO_2 outgassing occurs near the ACC where the intense vertical mixing increases the surface DIC and, hence, pCO_2. Strong westerly wind forcing also contributes to effective CO_2 outgassing adjacent to the ACC. Interestingly, the sign of the CO_2 flux changes near 55°S where the MLD abruptly shallows. The region north of that latitude takes up CO_2 from the atmosphere as pCO_2 becomes smaller than pCO_2^{atm}. Deep mixing can provide iron to the surface (Tagliabue et al., 2014) and promote biological drawdown that partially compensates the increase of the surface pCO_2, but its magnitude in our simulation is much less than that of DIC vertical flux because of light limitation in winter. Mesoscale eddies in the model simulations alter DIC concentration as shown in the fluctuating isolines of DIC and hence modulate CO_2 flux by perturbing the concentration of DIC. See Song, Marshall, Munro, Dutkiewicz, Sweeney, et al.(2016) for a detailed discussion of the modulation of CO_2 flux by the mesoscale.

2.3. Suppression of NIWs in the Biogeochemical Model

For the quantification of the impact by NIWs on air-sea CO_2 flux, we designed an offline simulation of the biogeochemical model with suppressed variances in time. This offline simulation (referred to as 5dAVG hereinafter) was integrated from the second year of ONLINE for 3 years driven by 5-day-averaged temperature (T), salinity (S), and horizontal velocities (U, V) from ONLINE. The vertical mixing for tracers was recalculated by the KPP scheme using those 5-day-averaged ocean states. The surface forcing is not changed in the surface mixing model and the biogeochemical model.

The 5-day average significantly suppresses processes with time scales shorter than a few days, and the spectral peak along f in the variances disappears (Figure 2b). Instead, almost all the energy in the vertical shear in 5dAVG is concentrated near zero-frequency-associated geostrophic currents. The 5-day average also slightly lowers the kinetic energy in the wavenumber band corresponding to the mesoscale (Figure 2c). However, the surface vorticity in 5dAVG shown in the inset of Figure 2c still shows rich structures associated with the mesoscale. The power density spectra of the square of the vertical velocity in 5dAVG are up to 100 times lower than ONLINE, but its power remains small ($O(10^{-5}\ m^2/s^2)$) compared with that in the lateral velocity (not shown). Hence, we can interpret the solution from this offline biogeochemical model as having a similar phenomenology as ONLINE except with reference to vertical mixing, which is much suppressed due to the lack of energy associated with NIWs.

As the focus of our study is on the impact of vertical mixing by NIWs on the CO_2 flux, we designed additional offline biogeochemical simulation where the vertical mixing (eddy diffusivity and eddy diffusivity weighted by nonlocal transport coefficient) from ONLINE were provided to the offline simulation. This offline simulation is referred to as CTRL hereinafter. This CTRL simulation then has the same mean physical oceanic states and surface vertical mixing as ONLINE, and the comparison of CTRL and 5dAVG allows us to isolate the impact of vertical mixing associated with NIWs on CO_2 flux. All three biogeochemical simulations are summarized in Table 1.

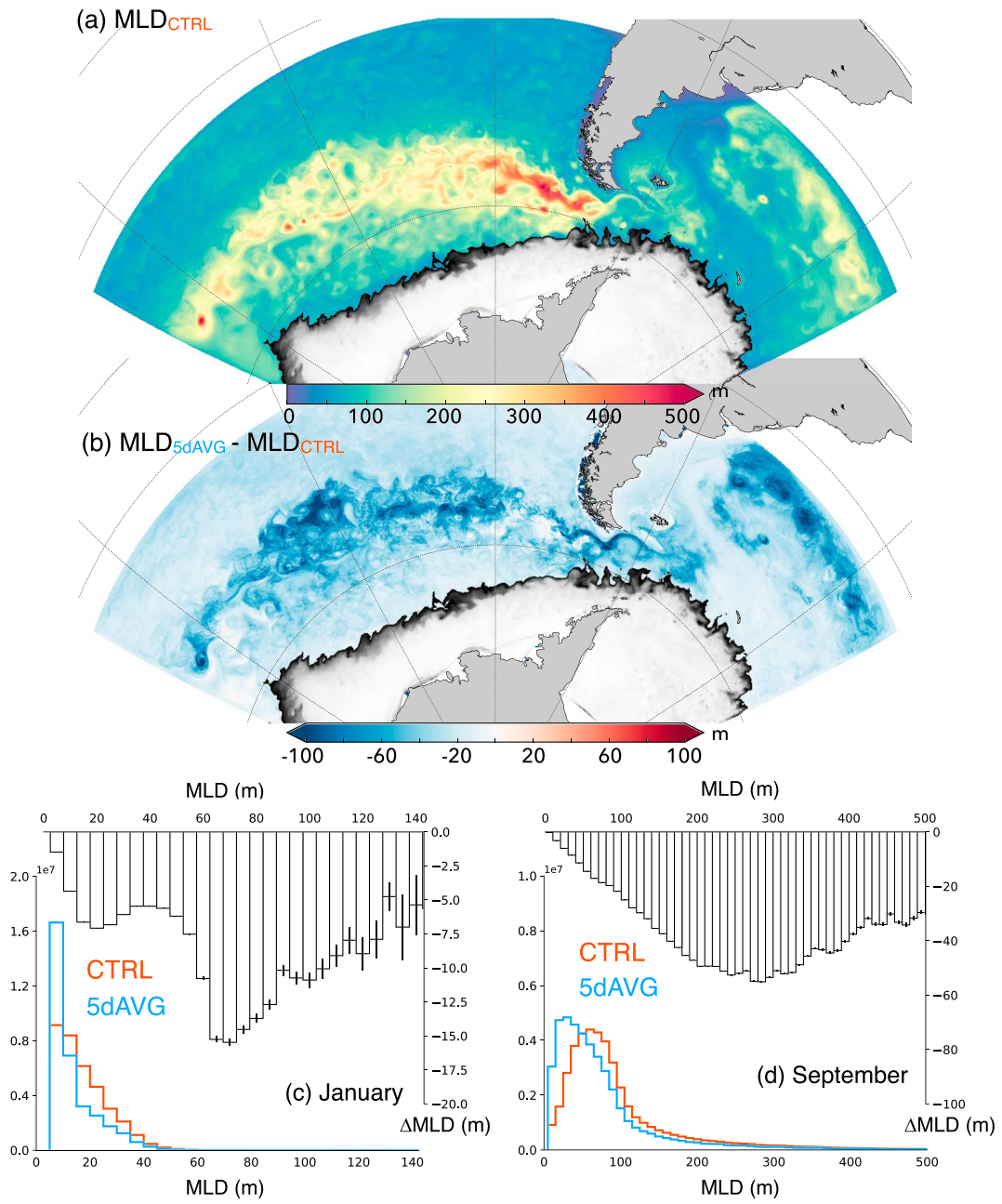

Figure 3. (a) Mixed layer depth (MLD) in the CTRL simulation averaged in September and (b) the changes in MLD between CTRL and 5dAVG. The mask in gray scale is the simulated sea ice fraction. Panels (c) and (d) are histograms of MLDs in CTRL (red) and 5dAVG (blue) in January and September, respectively, with the mean MLD differences (black bar plots) between the two runs binned by the original MLDs in CTRL. Black lines in the bar plots represent the standard errors. Note that the scales of the *x* and *y* axes are different between (c) and (d).

3. Impact of NIWs on MLD and Air-Sea CO_2 Fluxes

3.1. MLD

The CTRL run captures the observed wintertime MLD structure: MLDs reaching deeper than 500-m upstream of Drake Passage (Figure 1b) and relatively shallow MLDs of roughly 150 m in the Atlantic (Figure 3a; Dong et al., 2008; Holte et al., 2017; de Boyer Montégut et al., 2004). The absence of NIWs in 5dAVG reduces the vertical shear and weakens the vertical mixing, leading to shallower MLD. The reduction in MLD occurs almost everywhere, but it is more pronounced along the ACC where it can be greater than 100 m (Figure 3b). Since the MLD is an important factor in the calculation of eddy diffusivity in the KPP

scheme, one can expect to have larger changes in the eddy diffusivity along the ACC than in other areas. The maximum eddy diffusivity in 5dAVG is on average approximately 40% level that found in ONLINE along the ACC. The wintertime reduction in MLD is greater than in the summertime, which may be associated with the fact that midlatitude storms are important source for NIWs (Alford et al., 2016).

The reduction in MLD in 5dAVG can be further evaluated using histograms of MLDs. In January, the mean MLD in 5dAVG is 12.4 m (blue line in Figure 3c), about 5 m shallower than that in CTRL (red line in Figure 3c). The histogram of 5dAVG is shifted to the left and becomes more skewed: the moment coefficient of skewness is increased from 1.0 to 1.5 when the vertical mixing is recalculated using 5-day-averaged fields. We also computed the mean reduction of MLD after grouping the background MLD with the 5-m bins (the black bar plot in Figure 3c). All MLD ranges consistently show the reduction, indicating the systematic shoaling of the MLD. The size of MLD reduction increases with the background MLD in CTRL until 70 m, but decreases beyond that point. Similar patterns stand out in the MLD changes in September (Figure 3d). The mean MLD in 5dAVG is 83.5 m, which is roughly 24 m shallower than that in CTRL. The histogram of MLD in 5dAVG is more positively skewed than that in CTRL: the moment of coefficient of skewness in 5dAVG is 16.6 while it is 14.7 in CTRL. The reduction of MLD tends to increase as the background MLD becomes deeper, but it starts to decrease with the background MLD for bin sizes greater than roughly 300 m (the black bar plot in Figure 3d).

We argue that the reduction of MLD results from the elimination of vertical shear of the current in the near-inertial frequency band associated with NIWs (Figures 2a and 2b). The depth of the surface boundary layer in the KPP mixing scheme is defined as the level where the Richardson number is smaller than a predefined critical value. Since the Richardson number is inversely proportional to the vertical shear of the current, the decrease of vertical shear in 5dAVG can result in the increase of the Richardson number, and a reduction of the MLD and vertical eddy diffusivity. Just as temporal smoothing suppresses the kinetic energy, especially of the mesoscale (Figure 2b), it can alter the stratification near the surface. Suppose, for example, there is a cold eddy that moves along the current where stratification is roughly constant. Taking a 5-day average of the temperature has the effect of introducing cold (and thus heavy) water along the path over the 5-day span and thus might be expected to change the stratification and hence MLD. However, we find that the 5-day average has little impact on squared Brunt-Väisälä frequency (N^2) in the upper ocean (not shown), suggesting that the MLD reduction is driven mainly by the reduced level of vertical shear due to the absence of NIWs in 5dAVG.

3.2. Air-Sea CO_2 Flux

The CO_2 flux in ONLINE exhibits seasonal variability (red line in Figure 4a). In summer, the ocean takes up CO_2 from the atmosphere while the ocean emits CO_2 back to the atmosphere in winter. This is consistent with previous studies of air-sea CO_2 exchange in the SO (Lenton et al., 2013). In CTRL where the 5-day-averaged fields, including vertical mixing, drive the biogeochemical model, the ocean takes up more CO_2 in summer and releases more CO_2 in winter (green line in Figure 4a). Although the change in CO_2 flux can be as big as 0.1 Pg C/year, the mean difference is rather small (−0.04 Pg C/year), suggesting that CTRL is a realistic approximate to ONLINE. When the surface vertical mixing is recalculated using the 5-day-averaged fields in 5dAVG, the CO_2 uptake in summer is further enhanced while the outgassing of CO_2 in winter weakens (blue line in Figure 4a). The mean change in CO_2 flux in 5dAVG is −0.23 Pg C/year with respect to ONLINE and −0.19 Pg C/year with respect to CTRL, with the maximum reduction occurring in winter. The size of the CO_2 flux change in 5dAVG is considerable, having an amplitude of 30% of the seasonal cycle of CO_2 in ONLINE. It is also large when compared with the seasonal cycle of CO_2 in CTRL, roughly 20% of the level in CTRL.

Suppressing processes with high temporal frequency is responsible for the shift of the CO_2 flux curve from 5dAVG downward compared to that of ONLINE (Figure 4a). Because the surface wind is fixed and the mean temperature is the same, the downward shift of the CO_2 flux curve from 5dAVG is solely the result of the reduction in surface pCO_2. The impact of removing NIWs alone is quantified by comparing CTRL and 5dAVG simulations. The largest impact is observed in winter and spring, while the impact is minimum summertime. This seasonality in the impact of suppressed NIWs is to be expected, given that the main energy source for NIWs is the wind.

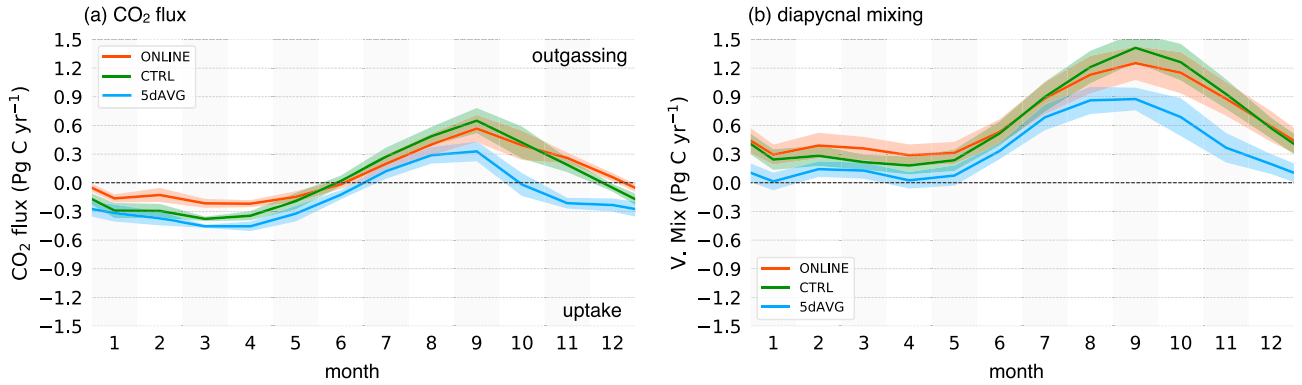

Figure 4. Area-integrated (a) CO_2 flux and (b) diapycnal mixing of dissolved inorganic carbon for each month from ONLINE (red), CTRL (green), and 5dAVG (blue).

To quantitatively investigate the drivers of CO_2 flux changes, we write the DIC concentration thus

$$\frac{\partial \mathrm{DIC}}{\partial t} = -\nabla \cdot (\mathbf{u}\mathrm{DIC} \quad) + \kappa \frac{\partial}{\partial z}\left(\frac{\partial \mathrm{DIC}}{\partial z}\right) - F_{\mathrm{CO}_2} + S_{\mathrm{bio}} + S_{\mathrm{C}}, \tag{2}$$

where $\mathbf{u}$ is a three-dimensional velocity vector, κ is the vertical diffusivity, F_{CO_2} is the CO_2 flux, and S_{bio} and S_{C} are the source/sink terms associated with biological activity and calcium carbonate flux, respectively. According to (2), the DIC tendency is determined by advection, diapycnal mixing and addition/subtraction of DIC through biogeochemical processes and air-sea exchange whose rate is determined by the ambient pCO_2 level through (1). When comparing the terms in ONLINE, CTRL, and 5dAVG, excluding F_{CO_2}, the biggest differences are found in $\kappa(\partial^2 \mathrm{DIC}/\partial z^2)$ (Figure 4b; other terms not shown). Clearly, the magnitude of the changes in diapycnal mixing is sufficient to explain the CO_2 flux changes, indicating that the supply of carbon-rich water from below through vertical mixing is the primary driver.

The changes in CO_2 flux have spatial structures (Figure 5), which resemble changes in the pattern of the vertical diffusive flux (Figure 6). In summer when most of the model domain takes up CO_2, the suppression of processes with high temporal variability allows the ocean to absorb more CO_2 near the ACC (Figure 5c). Because of CO_2 uptake, we find a weak vertical gradient of DIC near the surface (Figure S2 in the supporting information). In some locations along the ACC, it even becomes positive in which case the vertical diffusive flux of DIC is negative (Figure 6a). Since ONLINE and CTRL have the same mean state and vertical mixing, the differences in Figure 6c can be attributed to vertical diffusive flux of DIC associated with short timescale processes that are removed during the 5-day average and expressed as $\langle \kappa'(\partial \mathrm{DIC}/\partial z)' \rangle$. Episodic convection events in ONLINE can homogenize the DIC concentration near the surface layer, leading to a negative $\langle \kappa'(\partial \mathrm{DIC}/\partial z)' \rangle$ (Figure 6b) when $\langle \partial \mathrm{DIC}/\partial z \rangle$ is positive. Thus, one might expect higher pCO_2 at the surface and less CO_2 uptake in ONLINE than CTRL (Figure 5b).

If vertical mixing is recalculated using states without short timescale processes, further uptake of CO_2 occurs mainly near the ACC in summer (Figure 5e). These spatial changes are also closely linked to the changes in the mean vertical diffusive flux of DIC by diapycnal mixing expressed as $-\langle \kappa \rangle \langle \partial \mathrm{DIC}/\partial z \rangle$. 5dAVG has weaker mixing and $\langle \kappa \rangle$ has to be smaller than in CTRL, resulting in a reduction of carbon supply by vertical mixing when filtering out NIWs. The responses of the biological pump to suppressing high temporal variability and NIWs are not as large as those due to vertical mixing (not shown); hence, reduced supply of carbon from below leads to more uptake of CO_2 (Figures 4a and 5c and 5e).

In winter, using 5-day-averaged physical fields and eddy diffusivity in the biogeochemical model does not alter the CO_2 flux as much as in summer near the ACC. However, their impact is the opposite to that in summer (Figures 5b and 5d). In winter, the vertical diffusive flux of DIC is positive along the ACC, indicating that $\langle \partial \mathrm{DIC}/\partial z \rangle$ is negative. When episodic convection events homogenize the DIC concentration near the surface layer, $\langle \kappa'(\partial \mathrm{DIC}/\partial z)' \rangle$ becomes positive (Figure 6d). The biggest changes are observed in the Brazil-Malvinas confluence zone. Here there is originally CO_2 uptake in ONLINE (Figure 5b), but the positive difference between CTRL and ONLINE suggests that the CO_2 flux is close to zero or even positive

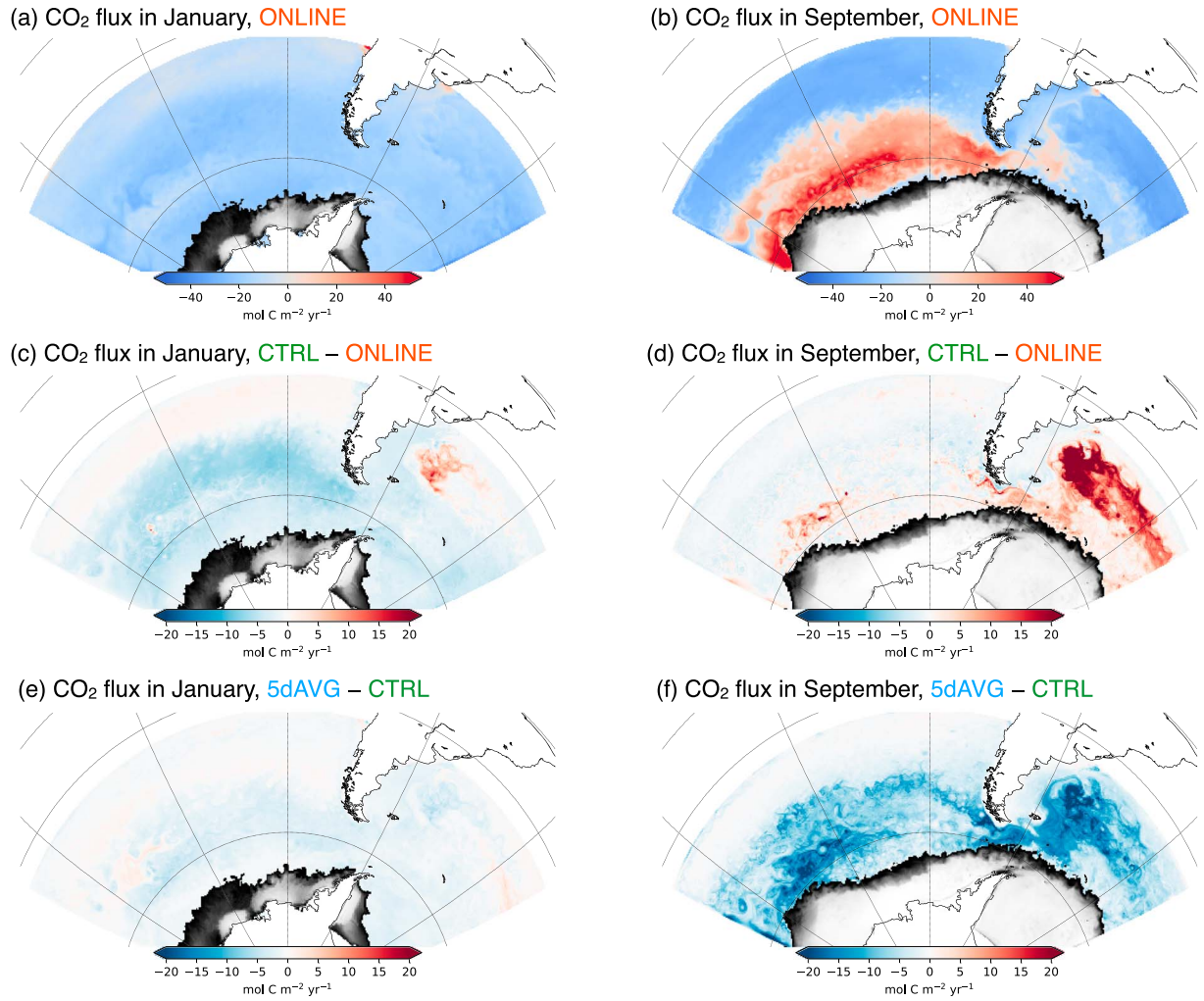

Figure 5. (a, b) Monthly averaged CO_2 flux in ONLINE, and (c, d) the difference between CTRL and ONLINE, and (e, f) between 5dAVG and CTRL. The panels on the left (a, c, and e) are the CO_2 flux and its difference in January, and the panels on the right (b, d, and f) are those in September. Similar to Figure 1, the gray mask near Antarctica represents the sea ice concentration.

(outgassing) after removing $\langle \kappa'(\partial \mathrm{DIC}/\partial z)' \rangle$ (Figure 5d). Although the main driving process is unclear, it is plausible that the larger vertical gradient of DIC in the zone can yield greater $(\partial \mathrm{DIC}/\partial z)'$ when homogenized by episodic convection events. Whatever the biggest changes in CO_2 flux in this zone between ONLINE and CTRL suggests that the effect of the high temporal processes is the greatest there.

In winter, suppressing NIWs reduces CO_2 outgassing (Figure 5f). Changes in the vertical diffusive flux of carbon can also explain the CO_2 flux changes between simulations in winter. The weakening of the vertical mixing in 5dAVG decreases $\langle \kappa \rangle$, and the vertical diffusive flux of DIC diminishes as expected (Figure 6f). The magnitude of the reduction in both vertical diffusive flux of DIC and CO_2 outgassing are much greater in winter than summer, which is consistent with the changes in MLD. These results point to the fact that the impacts of suppressing NIWs on the vertical mixing and resulting CO_2 flux change are greater in winter.

The results from ONLINE and 5dAVG demonstrate that suppressing NIWs and processes of high temporal variability shallows the MLD as shown in Figure 3. Since eddy diffusivity, κ, in the KPP scheme is proportional to the depth of surface boundary layer, it is the smallest in 5dAVG, leading to the weakest vertical diffusive flux of carbon to the surface. The decrease of carbon supply from subsurface lowers the pCO_2 at the surface and causes more uptake of CO_2 in summer and less CO_2 outgassing in winter. Driving the biogeochemical model with the same mean states including vertical mixing but without processes associated with high temporal variability (CTRL) also modifies the diffusive flux of carbon, lowering surface pCO_2 in

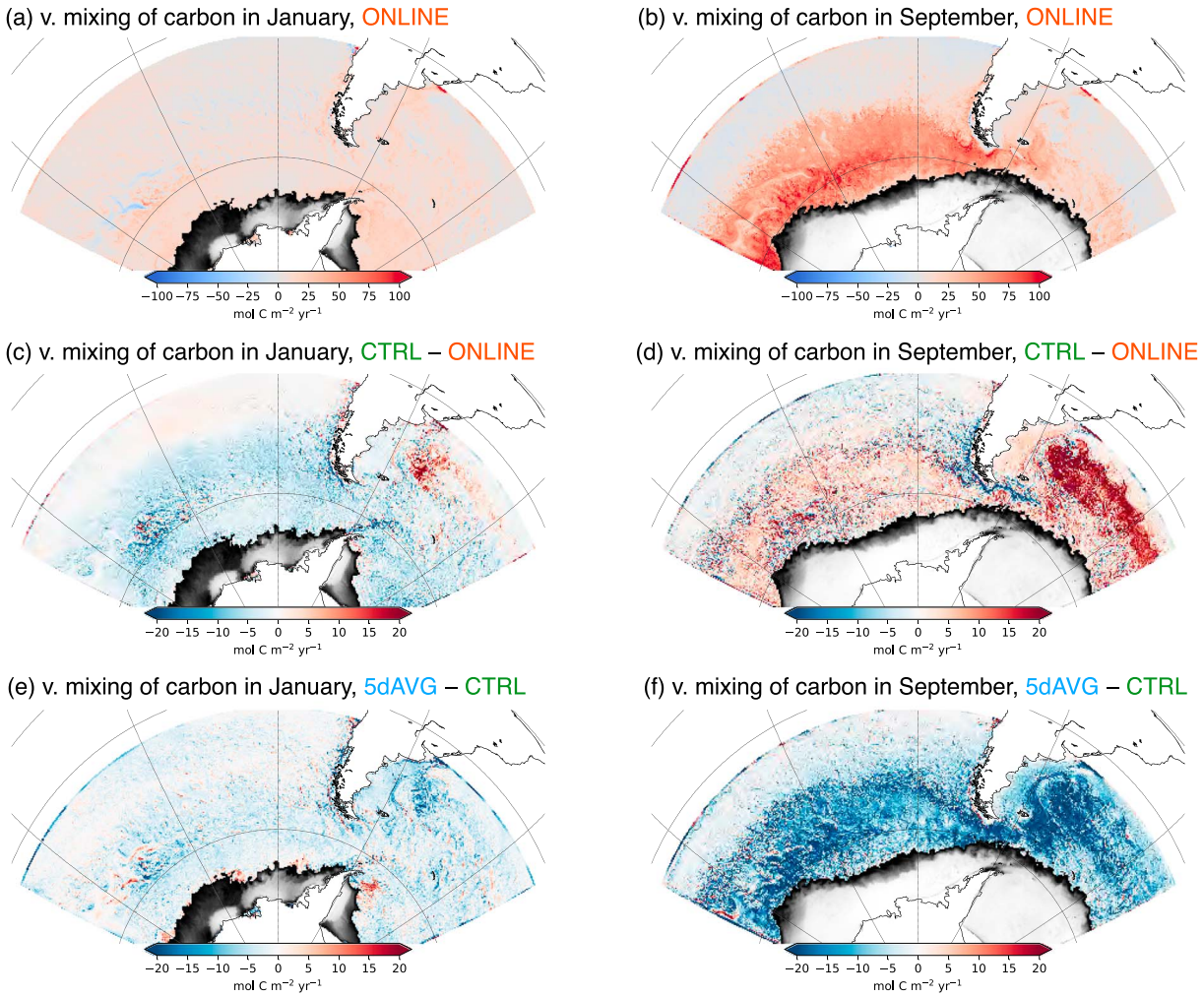

Figure 6. Same as Figure 5, but for the vertical mixing contribution to the surface dissolved inorganic carbon.

summer but increasing it in winter (Figures 4b and 6c and 6d). The effect of NIWs on CO_2 flux can be isolated by comparing CTRL and 5dAVG, and the comparison suggests that the effect of NIWs in CO_2 flux is greater in winter (Figures 4b and 6e and 6f). The decrease of carbon supply by vertical mixing can explain the reduced outgassing of CO_2 when NIWs are suppressed in winter (Figure 5f).

4. Discussion

Three numerical experiments demonstrate the sensitivity of air-sea CO_2 flux to high-frequency processes. Weakening of vertical mixing leads to less supply of carbon-rich water from below and reduces the surface carbon concentration. Budget analysis of DIC reveals that the vertical diffusive carbon flux is systematically lower when NIWs are suppressed (5dAVG; Figure 4b). As a result, the SO emits less CO_2 in austral winter and takes up more CO_2 in austral summer. Moreover, this change is approximately one third of the magnitude of the seasonal variability in ONLINE.

We note that removing NIWs and processes with high temporal variability can potentially affect the air-sea CO_2 exchange by changing the solubility of the surface ocean. Temporal smoothing reduces the warm/cold temperature anomalies and increases/decreases solubility, resulting in the decrease/increase of partial pressure of CO_2 that changes CO_2 flux. However, we expect this to result in a very small net effect. The temporal smoothing preserves mean properties; hence, there is no net sea surface temperature change. Since the changes in partial pressure of CO_2 with respect to temperature is fairly constant (Takahashi et al., 1993), net-zero temperature change should yield a very small net change in partial pressure of CO_2.

The 5-day average removes all processes with temporal scales shorter than a few days along with NIWs. Those processes can be important to explain changes in vertical mixing and CO_2 flux. In particular, the submesoscale cannot be neglected in the vertical processes affecting the surface pCO_2 and the carbon cycle. Because of its short length and time scales, the submesoscale demands a very high resolution simulation. Our numerical experiment with 1/20° resolution (ONLINE) has a chance to simulate the submesoscale, while 5dAVG does not. To find out whether ONLINE can simulate the submesoscale, we computed the Rossby number using a snapshot in winter. In most of the domain, the Rossby number is of $O(0.1)$ except for a few points mostly near the coast (Figure S3 in the supporting information). This is 1 order of magnitude smaller than the Rossby number typical of simulations, which resolve the submesoscale (McWilliams, 2016). It indicates that 1/20° resolution is still not high enough to explicitly resolve SO submesoscale processes (Rosso et al., 2014; Rosso et al., 2015). Hence, we conclude that the MLD changes in the 5dAVG is not associated with submesoscale in our experiment.

High-frequency wind forcing can change not only vertical mixing but also the ocean circulation itself. Duteil (2019) examines the oxygen concentration in the tropical Pacific Ocean after removing high frequency in the wind forcing and finds changes in ocean circulation and also oxygen concentration in subsurface regions (200–700 m), in addition to the shoaling of the MLD. The SO circulation might also be different if we exclude the high-frequency physical processes represented by NIWs. Thus, CO_2 flux could be influenced by both changes in mixing and ocean circulation. Since our experiments fix the mean ocean circulation and we are able to isolate the role of NIWs on surface mixing and the resulting CO_2 flux, our study can be useful to interpret the role of the changes in the ocean circulation on the CO_2 flux if one performs similar experiments as in Duteil (2019).

In nature, the effect of NIWs on vertical mixing and CO_2 flux may be greater than found in this study. Rimac et al. (2013) report that there is more than three times greater wind energy input to near-inertial motions by the hourly wind with 0.35° resolution than by 6-hourly wind with 1.875° resolution. Their result suggests that the 6-hourly wind whose resolution is close to 1° may not excite the NIWs fully in our experiment. Indeed, the amplitude of the energy near the inertial frequency in our study is on the order of 10^2 $cm^2 \cdot s^{-2} \cdot cpd^{-1}$ (Figure S1 in the supporting information), which is an order of magnitude smaller than the observations (Alford et al., 2016). If the wind product carried full energy associated with NIWs, the reduction of vertical mixing and the surface pCO_2 would be even more dramatic.

Here we have shown that processes with a high temporal frequency such as NIWs have a significant impact on vertical mixing and CO_2 flux, suggesting that such processes must be resolved in numerical simulations to improve estimation of the air-sea CO_2 flux in the SO. In order to properly simulate NIWs, the frequency of the wind forcing should be higher than the local inertial frequency. The inertial frequency increases with latitude, and is close to 2 cpd near −75°S, the southern boundary of our model (Figure 2a). At this latitude, at least 6-hourly winds are required to accurately force NIWs. However, many models do not use wind forcing with the frequency adequate for resolving NIWs, including those in the Coupled Model Intercomparison Project phase 5: Almost half of coupled climate models use only a daily coupling frequency (Tian, 2016). Even eddy-resolving models may miss the energy associated with NIWs if the wind forcing frequency is lower than local inertial frequencies.

Our study demonstrates that NIWs have broad impacts on both physical and biogeochemical properties. The impact is the strongest near the ACC in winter where many climate models show a shallow MLD bias (Downes et al., 2015). In recent years, the SO Carbon and Climate Observations and Modeling project deployed floats with the ability to estimate the carbon concentration at the surface and CO_2 exchange between the atmosphere and the ocean. The new observations revealed the wintertime CO_2 outgassing near the ACC (Gray et al., 2018), which had been underestimated by most numerical models. Hence it is important to evaluate whether NIWs are properly included in those numerical simulations in diagnosing the models' performance. Finally, we note that Hausmann et al. (2017) report on the modulation of MLD by mesoscale eddies in the SO, which is found to be significantly deeper in anticyclones, shallower in cyclones. One of the possible mechanisms could be preferential trapping of inertial waves in anticyclones, as has been discussed in, for example, Kunze (1985).

Acknowledgments
The MITgcm can be obtained from http://mitgcm.org website. Resources supporting this work were provided by the NASA High-End Computing (HEC) Program through the NASA Advanced Supercomputing (NAS) Division at Ames Research Center with the Award SMD-15-5752. H. S., J. M., and D. J. M. were supported by the NSF MOBY project (OCE-1048926 and OCE-1048897). H. S. acknowledges the support by National Research Foundation of Korea (NRF) grant (NRF-2019R1C1C1003663) and Yonsei University Research Fund of 2018-22-0053. D. J. M. also gratefully acknowledges NASA support.

References

Adcroft, A., Hill, C., Campin, J.-M., Marshall, J., & Heimbach, P. (2004). Overview of the formulation and numerics of the MIT GCM, *Proceedings of the ECMWF seminars on numerical methods (Recent developments in numerical methods for atmosphere and ocean modelling* (pp. 139–149). Shinfield Park, Reading, UK: ECMWF.

Adcroft, A., Hill, C., & Marshall, J. (1997). Representation of topography by shaved cells in a height coordinate ocean model. *Monthly Weather Review*, *125*, 2293–2315.

Alford, M. H., & Gregg, M. C. (2001). Near-inertial mixing: Modulation of shear, strain and microstructure at low latitude. *Journal Geophysical Research*, *106*(C8), 16,947–16,968. https://doi.org/10.1029/2000JC000370

Alford, M. H., MacKinnon, J. A., Simmons, H. L., & Nash, J. D. (2016). Near-inertial internal gravity waves in the ocean. *Annual Review of Marine Science*, *8*, 95–123. https://doi.org/10.1146/annurev-marine-010814-015746

D'Asaro, E. (1985). The energy flux from the wind to near-inertial motions in the mixed layer. *Journal of Physical Oceanography*, *15*, 1043–1059.

de Boyer Montégut, C., Madec, G., Fischer, A. S., Lazar, A., & Iudicone, D. (2004). Mixed layer depth over the global ocean: An examination of profile data and a profile-based climatology. *Journal Geophysical Research*, *109*, C12003. https://doi.org/10.1029/2004JC002378

Dong, S., Sprintall, J., Gille, S. T., & Talley, L. (2008). Southern Ocean mixed-layer depth from Argo float profiles. *Journal Geophysical Research*, *113*, C06013. https://doi.org/10.1029/2006JC004051

Downes, S. M., Farneti, R., Uotila, P., Griffies, S. M., Marsland, S. J., Bailey, D., et al. (2015). An assessment of Southern Ocean water masses and sea ice during 1988–2007 in a suite of interannual CORE-II simulations. *Ocean Modelling*, *94*, 67–94. https://doi.org/10.1016/j.ocemod.2015.07.022

Duteil, O. (2019). Wind synoptic activity increases oxygen levels in the tropical Pacific Ocean. *Geophysical Research Letter*, *46*, 2715–2725. https://doi.org/10.1029/2018GL081041

Dutkiewicz, S., Sokolov, A., Scott, J., & Stone, P. (2005). A three-dimensional ocean-sea ice-carbon cycle model and its coupling to a two-dimensional atmospheric model: Uses in climate change studies. *Joint program on the sci. policy global change* (Chap. Rep. 122 MIT, pp. 1–147). Cambridge, Mass.

Elipot, S., & Lumpkin, R. (2008). Spectral description of oceanic near-surface variability. *Geophysical Research Letters*, *35*, L05606. https://doi.org/10.1029/2007GL032874

Elipot, S., Lumpkin, R., Perez, R. C., Lilly, J. M., Early, J. J., & Sykulski, A. M. (2016). A global surface drifter data set at hourly resolution. *Journal Geophysical Research: Oceans*, *121*, 2937–2966. https://doi.org/10.1002/2016JC011716

Follows, M. J., Dutkiewicz, S., & Ito, T. (2006). On the solution of the carbonate system in ocean biogeochemistry models. *Ocean Modelling*, *12*, 290–301.

Gray, A., Johnson, K. S., Bushinsky, S. M., Riser, S. C., Russell, J. L., Talley, L. D., et al. (2018). Autonomous biogeochemical floats detect significant carbon dioxide outgassing in the high-latitude Southern Ocean. *Geophysical Research Letter*, *45*, 9049–9057. https://doi.org/10.1029/2018GL078013

Hausmann, U., McGillicuddy, D. J. Jr, & Marshall, J. (2017). Observed mesoscale eddy signatures in Southern Ocean surface mixed-layer depth. *Journal Geophysical Research: Oceans*, *122*, 617–635. https://doi.org/10.1002/2016JC012225

Holte, J., Talley, L. D., Gilson, J., & Roemmich, D. (2017). An Argo mixed layer climatology and database. *Geophysical Research Letter*, *44*, 5618–5626. https://doi.org/10.1002/2017GL073426

Jochum, M., Briegleb, B. P., Danabasoglu, G., Large, W. G., Norton, N. J., Jayne, S. R., et al. (2013). The impact of oceanic near-inertial waves on climate. *Journal Climate*, *26*, 2833–2844.

Kunze, E. (1985). Near-inertial wave propagation in geostrophic shear. *Journal of Physical Oceanography*, *15*, 544–565.

Large, W., McWilliams, J., & Doney, S. (1994). Oceanic vertical mixing: A review and a model with nonlocal boundary layer parameterization. *Reviews of Geophysics*, *32*, 363–403.

Lenton, A., Tilbrook, B., Law, R. M., Bakker, D., Doney, S. C., Gruber, N., et al. (2013). Sea-air CO_2 fluxes in the Southern Ocean for the period 1990–2009. *Biogeosciences*, *10*(6), 4037–4054. https://doi.org/10.5194/bg-10-4037-2013

Marshall, J., Adcroft, A., Hill, C., Perelman, L., & Heisey, C. (1997). A finite-volume, incompressible Navier Stokes model for studies of the ocean on parallel computers. *Journal Geophysical Research*, *102*(C3), 5753–5766.

Marshall, J., Hill, C., Perelman, L., & Adcroft, A. (1997). Hydrostatic, quasi-hydrostatic, and nonhydrostatic ocean modeling. *Journal Geophysical Research*, *102*(C3), 5733–5752.

Marshall, J., Jones, H., & Hill, C. (1998). Efficient ocean modeling using non-hydrostatic algorithms. *Journal of Marine Systems*, *18*, 115–134.

McWilliams, J. C. (2016). Submesoscale currents in the ocean. *Proceedings of the Royal Society A*, *472*(2189), 20160117.

Parekh, P., Follows, M. J., Dutkiewicz, S., & Ito, T. (2006). Physical and biological regulation of the soft tissue carbon pump. *Paleoceanography*, *21*, PA3001. https://doi.org/10.1029/2005PA001258

Rimac, A., von Storch, J. S., Eden, C., & Haak, H. (2013). The influence of high-resolution wind stress field on the power input to near-inertial motions in the ocean. *Geophysical Research Letter*, *40*, 4882–4886. https://doi.org/10.1002/grl.50929

Rosso, I., Hogg, A. M., Kiss, A. E., & Gayen, B. (2015). Topographic influence on submesoscale dynamics in the Southern Ocean. *Geophysical Research Letters*, *42*, 1139–1147. https://doi.org/10.1002/2014GL062720

Rosso, I., Hogg, A. M., Strutton, P. G., Kiss, A. E., Matear, R., Klocker, A., & van Sebille, E. (2014). Vertical transport in the ocean due to sub-mesoscale structures: Impacts in the Kerguelen region. *Ocean Modelling*, *80*, 10–23. https://doi.org/10.1016/j.ocemod.2014.05.001

Sasaki, H., Klein, P., Qiu, B., & Sasai, Y. (2014). Impact of oceanic-scale interactions on the seasonal modulation of ocean dynamics by the atmosphere. *Nature communications*, *5*, 5636.

Shao, A. E., Mecking, S., Thompson, L., & Sonnerup, R. E. (2013). Mixed layer saturations of CFC-11, CFC-12, and SF_6 in a global isopycnal model. *Journal Geophysical Research: Oceans*, *118*, 4978–4988. https://doi.org/10.1002/jgrc.20370

Simmons, H. L., & Alford, M. H. (2012). Simulating the long-range swell of internal waves generated by ocean storms. *Oceanography*, *25*(2), 30–41. https://doi.org/10.5670/oceanog.2012.39

Simmons, A., Uppala, S., Dee, D., & Kobayashi, S. (2007). ERA-Interim: New ECMWF reanalysis products from 1989 onwards, *ECMWF newsletter* (Vol. 110, pp. 25–35). ECMWF. https://doi.org.10.21957/pocnex23c6

Song, H., Marshall, J., Follows, M. J., Dutkiewicz, S., & Forget, G. (2016). Source waters for the highly productive Patagonian shelf in the southwestern Atlantic. *Journal of Marine Systems*, *158*, 120–128.

Song, H., Marshall, J., Gaube, P., & McGillicuddy, D. J. Jr (2015). Anomalous chlorofluorocarbon uptake by mesoscale eddies in the Drake Passage region. *Journal Geophysical Research: Oceans*, *120*, 1065–1078. https://doi.org/10.1002/2014JC010292

Song, H., Marshall, J., Munro, D. R., Dutkiewicz, S., Sweeney, C., McGillicuddy, D. J. Jr, & Hausmann, U. (2016). Mesoscale modulation of air-sea CO_2 flux in Drake Passage. *Journal Geophysical Research: Ocean*, *121*, 6635–6649. https://doi.org/10.1002/2016JC011714

Tagliabue, A., Sallée, J.-B., Bowie, A. R., Lévy, M., Swart, S., & Boyd, P. W. (2014). Surface-water iron supplies in the Southern Ocean sustained by deep winter mixing. *Nature Geoscience*, *7*, 314–320. https://doi.org/10.1038/ngeo2101

Takahashi, T., Olafsson, J., Goddard, J. G., Chipman, D. W., & Sutherland, S. C. (1993). Seasonal variation of CO_2 and nutrients in the high-latitude surface oceans: A comparative study. *Global Biogeochemical Cycles*, *7*(4), 843–878.

Takahashi, T., Sutherland, S. C., Wanninkhof, R., Sweeney, C., Feely, R. A., Chipman, D. W., et al. (2009). Climatological mean and decadal change in surface ocean pCO_2, and net sea-air CO_2 flux over the global oceans. *Deep-Sea Research Part II:*, *56*(8-10), 554–577.

Talley, L. D., Pickard, G., Emery, W., & Swift, J. (2011). *Descriptive physical oceanography: An introduction* (6th ed., pp. 560). Burlingham, MA: Elsevier.

Tian, F. (2016). Effects of coupling frequency on climate simulated by a coupled AO-GCM (PhD thesis). Hamburg: Max Planck Institute for Meteorology.

Tulloch, R., Ferrari, R., Jahn, O., Klocker, A., LaCasce, J., Ledwell, J., et al. (2014). Direct estimates of lateral eddy diffusivity upstream of Drake Passage. *Journal of Physical Oceanography*, *44*, 2593–2616.

Verdy, A., Dutkiewicz, S., Follows, M. J., Marshall, J., & Czaja, A. (2007). Carbon dioxide and oxygen fluxes in the Southern Ocean: Mechanisms of interannual variability. *Global Biogeochemical Cycles*, *21*, GB2020. https://doi.org/10.1029/2006GB002916

Wanninkhof, R. (1992). Relationship between wind speed and gas exchange over the ocean. *Journal Geophysical Research*, *97*(C5), 7373–7382. https://doi.org/10.1029/92JC00188

Wetzel, P., Winguth, A., & Maier-Reimer, E. (2005). Sea-to-air CO2 flux from 1948 to 2003: A model study. *Global Biogeochemical Cycles*, *19*, GB2005. https://doi.org/10.1029/2004GB002339